

## STATUS OF QCD

R. K. ELLIS

*Fermi National Accelerator Laboratory, P.O. Box 500,  
Batavia, IL 60510*

## ABSTRACT

Recent advances in perturbative QCD are reviewed. The topics discussed include structure functions, small  $x$  physics, direct photon production, heavy flavour production, jet physics and measurements of  $\alpha_s$ .

## 1. Structure functions

New data on deep inelastic structure functions have been presented in 1992 by the muon experiment NMC<sup>1</sup> and by the neutrino experiments CCFR<sup>2</sup> and FFMF.<sup>3</sup> Fig. 1 shows a comparison of the new muon scattering data with previous results from SLAC and BCDMS. The data interpolate nicely between the lower  $Q^2$  SLAC data and the BCDMS data. Also shown in Fig. 1 is the  $Q^2$  dependence of  $xF_3$  from the CCFR<sup>2</sup> and CDHSW<sup>4</sup> neutrino collaborations. The slope in  $Q^2$  differs between the two neutrino experiments; the CCFR data has a slope more consistent with QCD. The FFMF collaboration has about 100K events so the statistical precision is much less than the other two experiments.

Data with different beams and different isoscalar targets can be compared. This comparison has been performed, for example by Virchaux.<sup>5</sup> First, one must apply a correction for the beams, using the mean square charge relationship,

$$F_2^{p\pm}/F_2^{\nu N} = \frac{5}{18} \left(1 - \frac{6}{5} \frac{s - \bar{c}}{q + \bar{q}}\right) \quad (1)$$

Second, one should correct for nuclear effects using a parameterisation of the EMC effect.

The main conclusion to be drawn from this analysis is that the reanalysed EMC data<sup>6</sup> is in poor agreement with the other sets. In addition, there are less serious problems with low  $Q^2$  CDHSW data. The CCFR data interpolates nicely between the SLAC and BCDMS data. The overall conclusion is that there is now a precise set of structure function data from SLAC, BCDMS, NMC and CCFR which are in good mutual agreement. QCD fits lead to a value of  $\Lambda_{\overline{MS}} \approx 200$  MeV for four flavours. For a detailed discussion we refer the reader to the paper by Virchaux.<sup>5</sup>

1.1. Measurements at lower values of  $x$ 

The data from NMC also extends precise measurements to lower values of  $x$  than previously available. Fig. 2 shows the parton parameterizations of Martin, Roberts and Stirling<sup>7</sup> of 1990 ( $B_0$  and  $B_-$ ) and 1992 ( $D_0$ ) compared with the older BCDMS data as well with as the new NMC data. Fig. 2 makes clear the importance

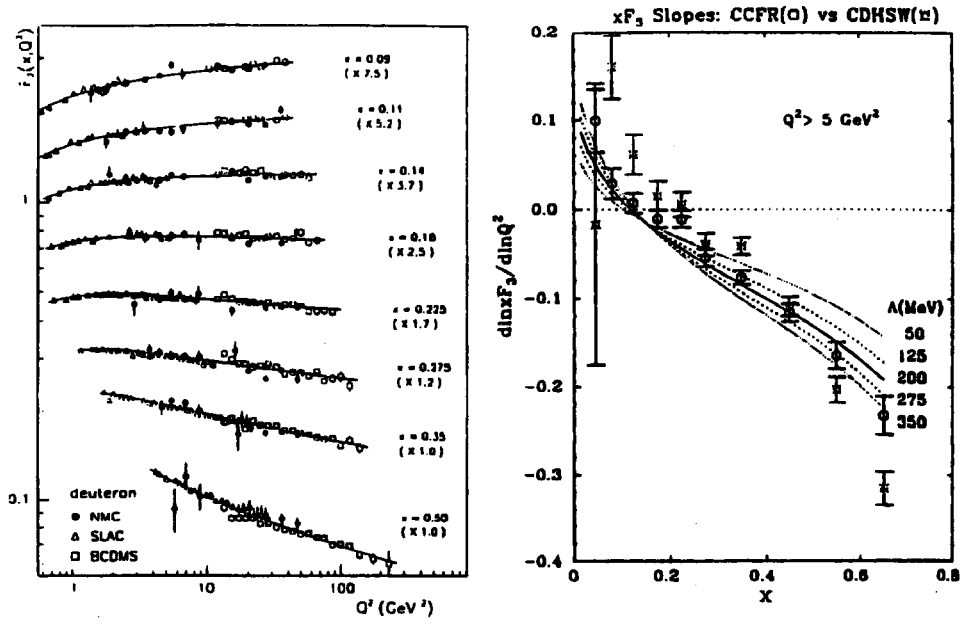


Figure 1: Comparison of lepton scattering experiments

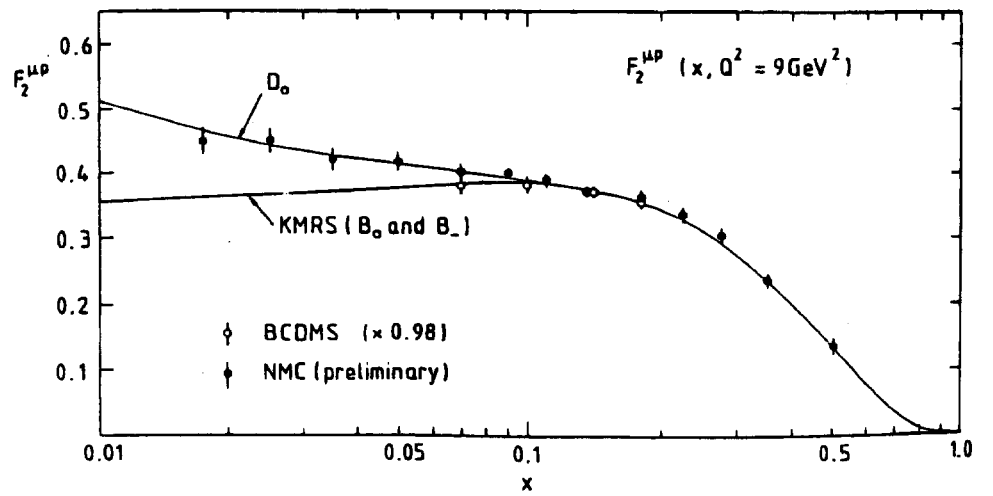


Figure 2: Comparison of NMC and BCDMS data with parton parameterizations

of experimental information in the low  $x$  region. Complete parton fits including the final NMC data are expected soon<sup>7,8</sup>.

The NMC results indicate that parton distributions should increase for  $x < 0.1$  as illustrated by Fig. 2. This change in parton distribution functions will have an impact on predictions for collider energies. At the Tevatron an object of mass 10 GeV is produced by partons with  $x \approx M/\sqrt{S} = 0.006$ . A  $W$  boson is produced at  $x \approx 0.05$ . Objects produced at large rapidities probe even lower values of  $x$ .

### 1.2. $SU(2)$ Symmetric Sea and the Gottfried Sum Rule

The NMC collaboration has also published information on the Gottfried sum rule.<sup>9</sup> The sum rule can be derived in the context of the quark parton model,

$$\int_0^1 \frac{dx}{x} (F_2^p - F_2^n) \equiv \frac{1}{3} \int_0^1 dx (u_v(x) - d_v(x)) - \frac{2}{3} \int_0^1 dx (\bar{d}(x) - \bar{u}(x)) \\ = \frac{1}{3} \text{ if } \bar{u} = \bar{d} \quad (2)$$

The NMC collaboration find

$$\int_{.004}^{0.8} \frac{dx}{x} (F_2^p - F_2^n) = 0.227 \pm 0.007 \pm 0.014 \quad (3)$$

The estimate of the value of the integral for all  $x$  is  $0.240 \pm 0.016$  which is significantly different from 0.33. To maintain  $\bar{u} = \bar{d}$ , the small  $x$  behaviour of the distributions must be modified to push the missing contribution into the unmeasured region. Simple ideas based on the Pauli principle give  $\bar{u} \neq \bar{d}$ . For a theoretical discussion of the Gottfried sum rule defect in the chiral quark model and references to earlier work, see Eichten et al.<sup>10</sup> Note that information on  $\bar{d} - \bar{u}$  can be obtained in a different  $x$  region from the nuclear target dependence of the  $x_F$  distribution in lepton pair production.<sup>11</sup>

### 2. Partons Distribution in the small $x$ Region

The physical picture of the gluon distribution is that  $xg(x, \mu^2)$  is the number of gluons per unit rapidity with transverse size less than  $1/\mu$  in a frame in which the hadron is fast moving. At small  $x$  it is also useful to define a more differential distribution of partons. The number of gluons with transverse momentum  $k_T$  and longitudinal fraction  $x$  is defined as  $f(x, k_T^2)$ . The normal gluon distribution is recovered by integrating over the transverse momentum up to scale  $\mu$ .

$$g(x, \mu^2) = \int_0^{\mu^2} dk_T^2 f(x, k_T^2) \quad (4)$$

There are three phenomena predicted theoretically in the small  $x$  region,

- 1.) Rapid growth of number of partons.
- 2.) Growth of mean transverse momentum in gluon cascade.
- 3.) Saturation phenomena.<sup>12</sup>

Fig. 3 gives a schematic map of the plane in  $x$  and  $Q^2$ . The evolution in  $Q^2$  is

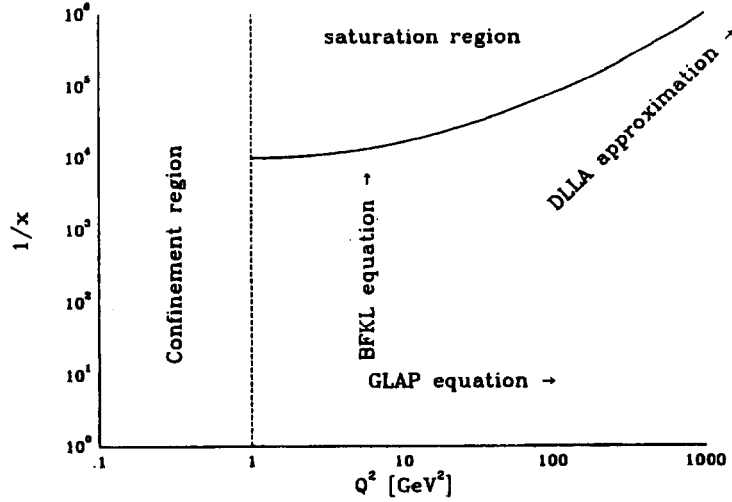


Figure 3: GLR plane showing the putative saturation region

controlled by the GLAP equation.<sup>13</sup> On the other hand the small  $x$  logarithms are resummed by the BFKL equation.<sup>14</sup> (For a unified treatment correct in both limits see the work of Marchesini and Webber<sup>15</sup>). If both  $\ln 1/x$  and  $\ln Q^2$  are large we may make a double leading logarithmic approximation (DLA) and both equations coincide. We begin by defining moments of the gluon distribution,

$$g(j, t) = \int_0^1 dx x^{j-1} g(x, t) \quad (5)$$

In terms of these moments the DLA of the Altarelli-Parisi equation for the gluon distribution  $g$  is,

$$\frac{dg(j, t)}{dt} = \frac{\bar{\alpha}(t)}{(j-1)} g(j, t), \quad \bar{\alpha} = \frac{N\alpha_s}{\pi} \quad (6)$$

where  $N = 3$ . The solution is

$$g(j, t) = g(j, t_0) \exp \frac{\xi}{b(j-1)}, \quad \xi = b \int_{t_0}^t dt' \bar{\alpha}_s(t') \sim \ln(\ln Q^2) \quad (7)$$

If both  $\xi$  and  $\ln 1/x$  are large, the inverse Mellin transform may be performed by saddle point methods,

$$xg(x, t) \sim \exp 2\sqrt{\frac{\xi \ln \frac{1}{x}}{b}} \quad (8)$$

The DLA teaches us that the gluon distribution grows very rapidly at small  $x$ . This feature is maintained in the full BFKL equation<sup>14</sup> which predicts a power growth at small  $x$ ,

$$xg(x, t) \sim \frac{1}{x^{j_1}}, \quad j_1 \sim 0.5 \quad (9)$$

Experiment	$\sqrt{s}$ [GeV]	$x$ -range
WA70	22	$0.35 < x_T < 0.55$
E706	31.5	$0.3 < x_T < 0.5$
UA1/UA2	630	$0.03 < x_T < 0.16$
CDF/D0	1800	$0.016 < x_T < 0.1$

Table 1:  $x$ -ranges probed by direct photon experiments

For inclusive quantities it is hard to distinguish this behaviour from the growth predicted by the GLAP equation. Methods of disentangling this behaviour from Altarelli-Parisi growth have been suggested in the literature.<sup>16</sup> The DLLA also teaches us that the important variables are  $\ln 1/x$  and  $\xi \equiv \ln \ln Q^2$ . In practical situations  $\ln 1/x$  is often much bigger than  $\xi$ . Thus from a practical point of view it is more important to understand small  $x$  than large  $Q^2$ .

The critical line shown in Fig. 3 is the line of constant packing fraction of partons. It corresponds to the start of parton interactions and the onset of saturation. The approach to this line from the perturbative region is governed by the equation<sup>17</sup> ( $G(x, Q^2) \equiv xg(x, Q^2)$ )

$$\frac{\partial^2 G(x, Q^2)}{\partial \ln 1/x \partial \ln Q^2} = \bar{\alpha}_s G(x, Q^2) - \frac{81}{16} \alpha_s^2 \frac{(G(x, Q^2))^2}{Q^2 R^2} \quad (10)$$

The second term slows the growth of the parton distribution and leads to a saturation of the parton density. The observability of saturation effects<sup>18</sup> depends on the value for  $R$ . A uniform distribution of partons corresponds to  $R \sim 1 \text{ fm} \sim 5 \text{ GeV}^{-1}$ . If the partons are clustered in hot spots a value of  $R \sim 0.2 \text{ fm} \sim 2 \text{ GeV}^{-1}$  would be more appropriate. The theoretical status of this equation, including the first demonstration in QCD that the terms which are formally 'power suppressed' will dominate the leading terms at small  $x$ , has been reviewed by Levin.<sup>19</sup>

### 3. Direct Photon Production

Direct photon production offers a clean way of probing the gluon distribution function in a limited range of  $x_T$ . The  $x_T$  ranges measured by selected present experiments are shown in Table 1. A fairly large coverage in  $x_T$  is now available. Results from experiment E706 investigating direct photon production with 500 GeV pion and proton beams have been presented by Dunlea.<sup>20</sup> Some deviations from current fits of structure functions are observed at low  $p_T$ . At collider energy we must impose an isolation cut to remove bremsstrahlung contributions. The theoretical understanding of this process has been reviewed by Qiu.<sup>21</sup> Fig. 4 shows the data from the Tevatron collider<sup>22</sup> compared to the most recent theoretical predictions.<sup>23</sup> The preliminary analysis of the D0 collaboration is in agreement, within errors, with the published CDF results. Note that the theoretical predictions,<sup>23</sup> using modern structure functions, give a reasonable description of the data for both large and small  $p_T$ .

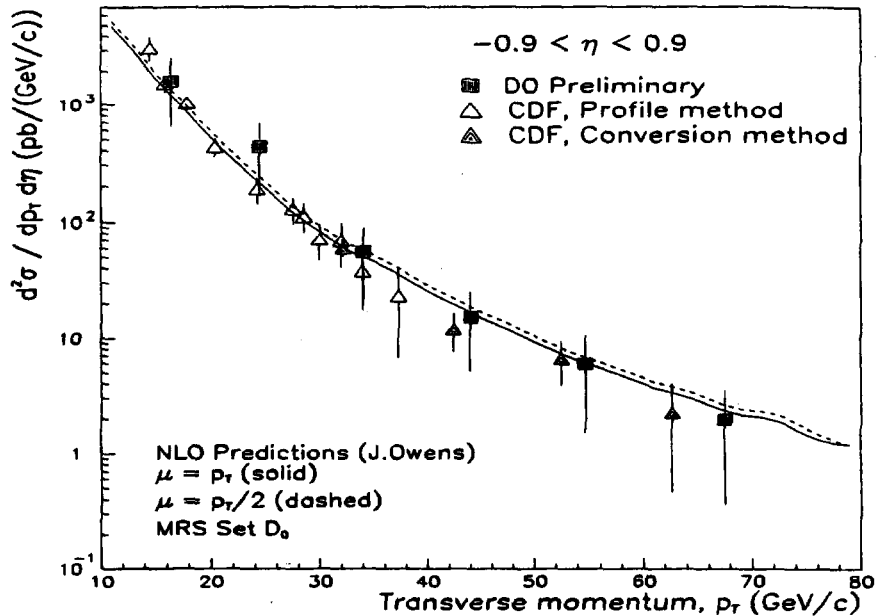


Figure 4: Tevatron results on direct photon production

#### 4. Heavy Quark Production

Heavy quark production proceeds both by the annihilation of a light quark with a light antiquark and by gluon-gluon fusion. Cross sections for the production of hadrons containing heavy quarks are calculable in the quark parton model. The large parameter which makes perturbation theory applicable is  $m_Q$ , the mass of the heavy quark. Corrections to the QCD parton model are of order  $\Lambda/m_Q$ .

##### 4.1. Production of hadrons containing charmed quarks

The mass of the charmed quark is such that the description of charmed hadron production using the heavy quark formalism is marginal. The production of charmed hadrons is interesting precisely because of the ambiguous nature of the charmed quark on the border between heavy and light quark.

At fixed target energies the theoretical prediction for total rate of charmed hadron production is extremely sensitive to the value chosen for the charm quark mass,  $m_c$ . By choosing plausible values of the charm quark mass, agreement can be found with the more recently measured values of total production cross-sections.<sup>25</sup> Measured differential cross sections for charmed *mesons* are in agreement with theoretical predictions for charmed *quarks*. There is no experimental evidence for the softening expected from fragmentation.

The evidence for a strong leading particle effect<sup>26</sup> is not confirmed by a

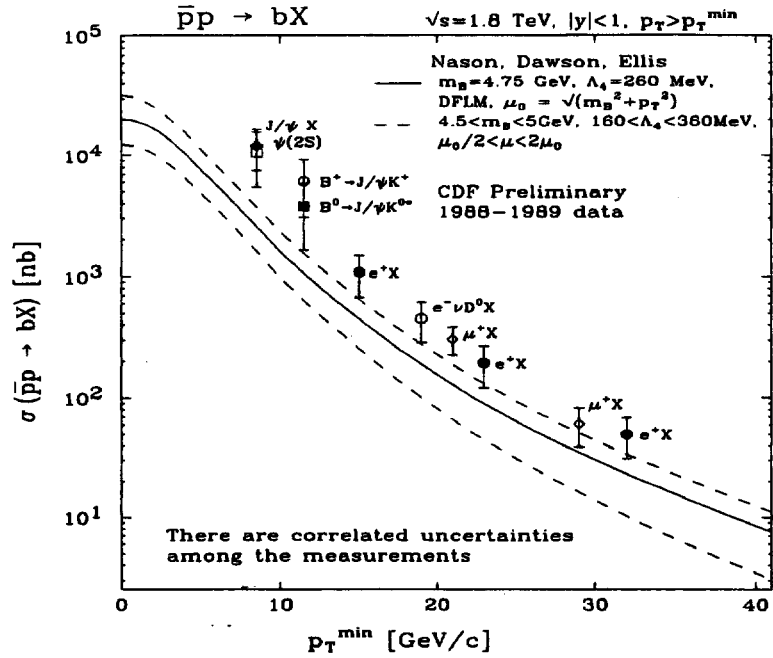


Figure 5:  $b$  quark production

higher statistics experiment.<sup>27</sup> A pronounced leading particle effect would indicate interaction between the remnants of the beam and the produced charmed quark to alter the  $x_F$  distribution. The Feynman  $x_F$  distributions for the  $D$ -mesons produced in the reaction  $\pi^- N \rightarrow D^\pm$  can be fitted to the form  $(1-x_F)^{n_\pm}$ . The measured value<sup>27</sup> of the difference of the exponents for the two types of mesons is  $n_+ - n_- = 1.1 \pm 0.4$ .

#### 4.2. Production of hadrons containing bottom quarks

The data on bottom production<sup>28</sup> at  $\sqrt{s} = 1.8 \text{ TeV}$  is shown in Fig. 5. The data lies above the band of theoretical predictions derived from  $\alpha_s^3$  theory,<sup>29</sup> unlike the corresponding data from UA1 at  $\sqrt{s} = 0.63 \text{ TeV}$ .<sup>30</sup> However several caveats are important in making this determination from Fig. 5. First, there is a large amount of manipulation of the data which goes into the determination of the bottom quark  $p_T$  distribution shown in Fig. 5. On the theoretical side the value of  $x$  at which the gluon distribution is probed is very small and the gluon distribution is not measured at such small values of  $x$ . In fact, one mechanism to accommodate the data shown in Fig. 5 is to alter the form of the gluon distribution.<sup>31</sup>

However the order  $\alpha_s^3$  theory is flawed for bottom production at  $\sqrt{s} = 1.8 \text{ TeV}$ . The order  $\alpha_s^3$  terms are equal in magnitude to the cross section predicted at the Born graph level ( $\alpha_s^2$ ). Thus the perturbation series for bottom production at the Tevatron is not stable order-by-order. The reason for the large correction is understood. It is due to the fact that  $\sqrt{s} \gg m \gg \Lambda$ . An improved theory of this regime has yet to be

worked out to the level of reliable numerical predictions. I shall try and describe the concepts required to give a description of this regime. For simplicity, consider the photoproduction of heavy quarks, since this process involves primarily photon-gluon fusion with only one gluon in the initial state.

In the standard parton model the cross section is schematically given by the product of the parton distribution and the on-shell cross section.

$$\sigma^{\gamma N} = \int_0^{m^2} dk_T^2 f(x, k_T^2) \otimes \hat{\sigma}(m^2) \equiv g(x, m^2) \otimes \hat{\sigma}(m^2) \quad (11)$$

In the region  $\sqrt{s} \gg m \gg \Lambda$ , the perturbation series is no longer a series in  $\alpha_s$ , but rather in  $\alpha_s \ln s/m^2$ . The transverse momentum of the incoming partons is no longer limited and a description in terms of an on-shell cross section is no longer appropriate. The modified form requires an off-shell cross-section (impact factor) and a distribution of gluons in  $x$  and  $k_T$ .

$$\sigma^{\gamma N} = \int_0^\infty dk_T^2 f(x, k_T^2) \otimes \hat{I}(k_T^2, m^2), \quad \hat{I}(0, m^2) = \hat{\sigma}(m^2) \quad (12)$$

How numerically important is the effect of off-shellness at practical energies<sup>32,35</sup>? The answer to the question depends on the importance of the tail region. This depends on the shape of the impact factor  $I$  as well as on the  $k_T$  behaviour of  $f(x, k_T^2)$ . The fact that the  $\alpha_s^2$  corrections to bottom production are large shows that these effects are important in fixed order calculations at present energies.

#### 4.3. Top Quark Production at Tevatron

The dominant parton process in top quark production at the Tevatron depends on the mass of the top quark,  $m_t$ . If  $m_t \sim 100$  GeV then the  $gg \rightarrow Q\bar{Q}$  and  $q\bar{q} \rightarrow Q\bar{Q}$  processes are of equal importance. For  $m_t > 100$  GeV the process  $q\bar{q} \rightarrow Q\bar{Q}$  dominates because of the stiffer quark distributions. Note that  $W$  gluon fusion does not lead to an observable signal<sup>36</sup> in 100 pb<sup>-1</sup> samples at  $\sqrt{s} = 1.8$  TeV. Thus the phenomenological parameters required to predict the rate of top quark production are the quark distribution at  $x \sim 0.1$  and the value of  $\alpha_s$ . There are various levels of sophistication with which we can calculate top quark cross sections. Including the  $\alpha_s^2$  corrections leads to a reduction in theoretical error,<sup>33</sup> when compared with tree graph level calculations. A partial resummation of higher order terms<sup>34</sup> indicates a further 10% increase. Including all known effects a reasonable estimate of the theoretical error on the top cross-section is that it is determined to  $\pm 20\%$ .

We now consider the background which can mask the top quark signal. One of the most important applications of the multi-jet calculations is the estimate of the background to the top quark search. A  $t\bar{t}$  event gives rise to an observable  $W + n$ -jet signature ( $n \leq 4$ ) when one of the  $W$ 's from top decay undergoes a semileptonic decay. The background is due to the production of a  $W$  in association with QCD jets. Fig 6 shows the cross-section for both as a function of the top quark mass.<sup>35</sup> Both the signal and the background are calculated at tree graph level. The jets are defined using standard cuts of the CDF collaboration (for details see Berends et

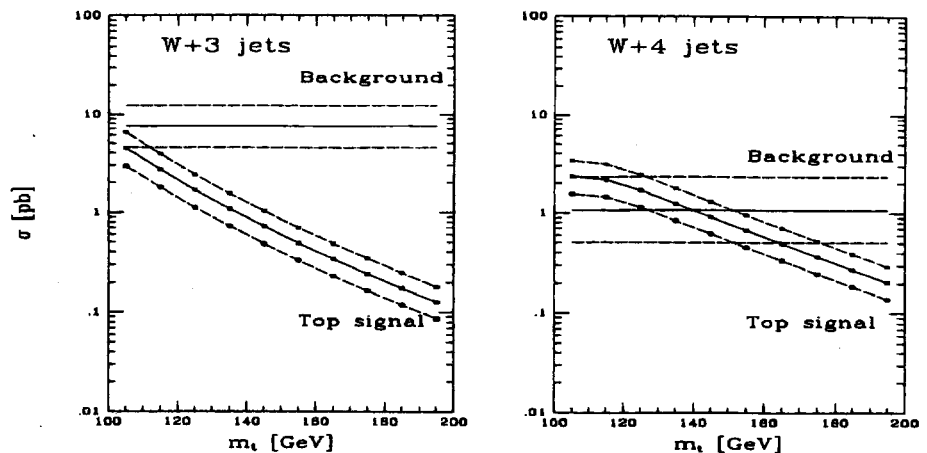


Figure 6:  $W + \text{jet}$  cross sections from background and signal

al.<sup>35</sup>). The theoretical uncertainty is estimated by varying the renormalisation scale between  $m_t/2 < \mu < 2\sqrt{(m_t^2 + p_T^2)}$  for the signal and between  $M_W/2 < \mu < 2\sqrt{(M_W^2 + p_T^2)}$  for the background. This plot shows the importance of the four jet channel for top discovery. Note however that these plots do not include the discrimination against the background obtained when a  $b$ -quark is identified. With  $b$  tagging, the  $W+4$  jets background is effectively removed.

The top quark cross sections are known beyond the leading order.<sup>33</sup> This allows us to reduce the theoretical error on the top quark cross section shown in Fig. 6. The upper values of the top quark cross sections shown in Fig. 6 are favoured by NLO calculations.

## 5. Jets

Tree level predictions for jet cross sections suffer from a number of deficiencies. First, they have no parton merging cone size dependence. The number of partons in the final state determines the number of jets. Two partons which are produced close together can never be merged to give a single jet. At tree level a single parton is equivalent to a jet. Second, they are sensitive to variations of the size of the coupling constant  $\alpha_s$ , and to the choice of renormalisation scale. This is particularly true of cross-sections which begin in order  $\alpha_s^n$  for large  $n$ . For example the  $W$  plus four jet cross section occurs in order  $\alpha_s^4$ . A 20% uncertainty in  $\alpha_s$ , coming from scale uncertainty and uncertainty in  $\alpha_s$ , itself, leads to a factor 2 uncertainty in the cross section. Estimates beyond leading order can be done either using a parton shower Monte-Carlo program or using fixed order perturbation theory. Both methods have their advantages. Here I describe only advances in fixed order techniques.

In fixed order perturbation theory one can sensibly define a cross section for any ‘infra-red safe’ quantity. This is technically complicated because it requires regulation and cancellation of contributions from real and virtual emission graphs,

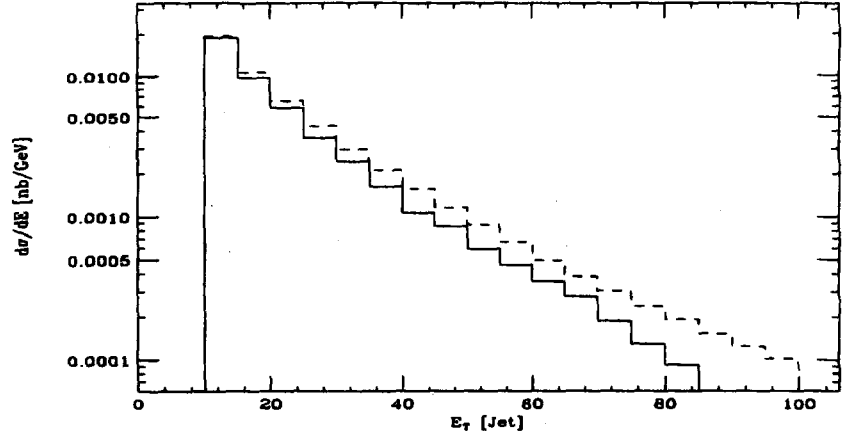


Figure 7: The  $W^\pm + 1$  jet cross section vs. the transverse energy of the jet. The dashed line is leading order, the solid line is next to leading order.

but presents no conceptual difficulties. Several calculations of jet cross-sections are now available beyond leading order.<sup>37</sup> Fig. 7 shows an example of such a calculation<sup>38</sup> for a  $W + 1$  jet cross-section plotted as a function of  $E_T$ . Standard CDF cuts are used. The softening of the jet  $E_T$  spectrum beyond the leading order is due to the use of a fixed  $E_T$  cut to define the jets. At high transverse energy the accompanying soft radiation scales with  $E_T$ . Thus at higher  $E_T$  the accompanying soft radiation is much more likely to promote the event to the two jet sample, leading to a smaller  $W + 1$  jet sample.

## 6. The measurement of $\alpha_s$

### 6.1. $\alpha_s$ at low $Q^2$

If measurements of  $\alpha_s$  can be performed at low energy they can be competitive with high energy measurements. A 10% measurement of  $\alpha_s$  at 1.7 GeV corresponds to a 4% measurement at the mass of the  $Z$ , because of the focussing effect in the evolution of the coupling constant. Remarkably, it appears that the hadronic width of the  $\tau$  is able to provide a believable low energy measurement<sup>40</sup> of  $\alpha_s$ . The measurement begins with the ratio of the hadronic to leptonic decay widths of the  $\tau$  which is given theoretically by,

$$R_\tau = \frac{\Gamma(\tau \rightarrow \text{Hadrons})}{\Gamma(\tau \rightarrow e)} = 3S_{EW}(1 + \delta_{PQCD} + \delta_{NPQCD}) \quad (13)$$

$S_{EW} = 1.0194$  is a known electroweak correction.<sup>41</sup> The perturbative contribution  $\delta_{PQCD}$  is known up to third order.<sup>42</sup>

$$\delta_{PQCD} = a + 5.2a^2 + 26.4a^3 (\pm 130a^4), \quad a = \frac{\alpha_s(m_\tau)}{\pi} \quad (14)$$

The fourth order contribution (in brackets) shows the value chosen by Braaten et al.<sup>40</sup> to estimate the size of error in the estimate of  $\delta_{PQCD}$ . Since  $a$  will turn out to

be about 0.1 it is easy to check the size of the various contributions to  $\delta_{PQCD}$ . The non-perturbative corrections have also been estimated<sup>40</sup> and are found to be small, because of the absence of  $1/m^2$  terms in the limit of zero quark masses.

$$\delta_{NPQCD} = -0.007 \pm 0.004 \quad (15)$$

Thus the unknown higher order contributions to  $\delta_{PQCD}$  are largest source of theoretical uncertainty. The experimental measurement of  $R_\tau$  can be derived either from the lifetime measurement,  $1/\Gamma(\tau)$ , and the calculated leptonic widths of the  $\tau$ ,

$$R_\tau^\Gamma = \frac{\Gamma(\tau) - \Gamma(\tau \rightarrow e) - \Gamma(\tau \rightarrow \mu)}{\Gamma(\tau \rightarrow e)} \quad (16)$$

or from the leptonic branching ratios

$$R_\tau^B = \frac{\Gamma(\tau) - \Gamma(\tau \rightarrow e) - \Gamma(\tau \rightarrow \mu)}{\Gamma(\tau \rightarrow e)} = \frac{1}{B_e} - 1.973 \quad (17)$$

The 1992 results for these two independent determinations are<sup>43</sup>

$$\begin{aligned} R_\tau^\Gamma &= 3.55 \pm 0.06 \\ R_\tau^B &= 3.63 \pm 0.03 \end{aligned} \quad (18)$$

Note that with the recent measurements of the  $\tau$  mass and lifetime there is no longer a significant discrepancy between these two determinations and it is appropriate to average them to give  $R_\tau = 3.62 \pm 0.03$ . The value of the strong coupling derived from this average value is

$$\alpha_s(M_\tau) = 0.36 \pm 0.03 \rightarrow \alpha_s(M_Z) = 0.122 \pm 0.004 \quad (19)$$

A comparison with other determinations of  $\alpha_s$  is given later.

#### 6.2. $\alpha_s$ from $1P - 1S$ splitting in charmonium

The determination of  $\alpha_s$  from the  $1P - 1S$  splitting in charmonium<sup>44</sup> using lattice methods requires three steps. First, the determination of the lattice spacing in physical units using the measured spin splitting in the charmonium system; second, the determination of the physical coupling at a scale measured in lattice units; third, a correction for the absence of light quarks. The correction for the absence of light quarks, which is made using a QCD based potential model, is the largest source of uncertainty. It is argued that the use of the static potential is an acceptable procedure for the correction because it gives a good description of the charmonium system. When lattice calculations are performed in the future with dynamical fermions this correction will no longer be necessary. The value and estimate of the systematic error are

$$\alpha_s(5GeV) = 0.174 \pm 0.012 \rightarrow \alpha_s(M_Z) = 0.105 \pm 0.004 \quad (20)$$

### 6.3. Jet structure in $e^+e^-$ annihilation

Determinations of  $\alpha_s$  are now available using event shape variables and the high statistics data obtained at the  $Z$  pole at LEP. A complete review of these analyses is inappropriate here and we refer the reader to reviews by Bethke.<sup>45</sup> The connection between the perturbative results and the quantities derived from the hadrons measured experimentally is made by performing hadronisation corrections. The hadronisation corrections are examined by considering a series of Monte Carlo models. These corrections are nominally of order  $\Lambda/Q$ , but in practice are often found to be of order 10% or larger at LEP energies. The size of the hadronisation correction depends on the particular observable. Consider the perturbative expansion for a physical observable used to measure  $\alpha_s$ ,

$$O = \alpha_s(1 + \sum c_n \alpha_s^n) \quad (21)$$

with coefficients  $c_n$  assumed to be of order 1. The coefficient  $c_1$  is known, but  $c_2$  is not yet calculated. Thus the first perturbative correction term is about 10% at LEP energies, comparable in size to the hadronisation correction. The statement that the dominant error on an  $\alpha_s$  determination comes from ignorance of higher order terms such as  $c_2$ , depends on the estimate of the error on the hadronisation corrections from Monte Carlo programs. Note that despite the high energy the power suppressed terms play a more important role than in an inclusive measurement such as  $\tau$  decay.

### 6.4. Jet clustering algorithms and resummation

Jet cross sections in  $e^+e^-$  annihilation are defined in terms of a jet resolution parameter  $y_{cut}$  and a jet recombination scheme. In the original JADE algorithm the resolution parameter is taken to be  $M_j^2/Q^2$  where  $M_j$  is the maximum jet invariant mass. Thus in the Jade algorithm, we define,

$$y_{ij} = \frac{2E_i E_j (1 - \cos \theta_{ij})}{Q^2} \quad (22)$$

The algorithm then proceeds as follows

- 1.) Compute  $y_{ij}$ 's
- 2.) Define the smallest  $y_{ij}$  to be  $y_{kl}$ ; If  $y_{kl} < y_{cut}$ , form  $p_{kl} = p_k + p_l$
- 3.) repeat until all  $y_{ij} > y_{cut}$

Unfortunately this algorithm generates strong kinematic correlations and leads to a non-intuitive classification of some events. As a consequence, the resummation of large logarithms of  $y_{cut}$  appears theoretically hopeless in this scheme since exponentiation fails at leading log level. The modified  $k_T$  (Durham) algorithm<sup>46</sup> replaces Eq. (22) by

$$y_{ij} = 2(1 - \cos \theta_{ij}) \min(E_i^2, E_j^2) / Q^2 \simeq \frac{k_{ij}^2}{Q^2} \quad (23)$$

This modified algorithm is easier to treat theoretically, and predictions which resum leading and subleading logarithms have been given. Resummed calculations are available for jet rates in this scheme, as well as for thrust, heavy jet-mass and

Process	Q [GeV]	$\alpha_s(Q)$	$\alpha_s(M_Z)$	$\Delta\alpha_s(M_Z)$		Theory
				exp.	theor.	
$R_r$	1.77	$0.360 \pm 0.03$	$0.122 \pm 0.004$	0.002	0.004	NNLO
DIS [ $\nu$ ]	5.0	$0.193 \pm \begin{smallmatrix} 0.019 \\ 0.018 \end{smallmatrix}$	$0.111 \pm 0.006$	0.004	0.004	NLO
DIS [ $\mu$ ]	7.1	$0.180 \pm 0.014$	$0.113 \pm 0.005$	0.003	0.004	NLO
$c\bar{c}$ mass splitting	5.0	$0.174 \pm 0.012$	$0.105 \pm 0.004$	0.000	0.004	LGT
$J/\Psi + \Upsilon$ decays	10.0	$0.167 \pm \begin{smallmatrix} 0.015 \\ 0.011 \end{smallmatrix}$	$0.113 \pm \begin{smallmatrix} 0.007 \\ 0.005 \end{smallmatrix}$	0.001	$\pm \begin{smallmatrix} 0.007 \\ 0.005 \end{smallmatrix}$	NLO
$e^+e^-$ [ $\sigma_{had}$ ]	34.0	$0.157 \pm 0.018$	$0.131 \pm 0.012$	-	-	NNLO
$e^+e^-$ [ev. shapes]	35.0	$0.14 \pm 0.02$	$0.119 \pm 0.014$	-	-	NLO
$e^+e^-$ [ev. shapes]	58.0	$0.130 \pm 0.008$	$0.122 \pm 0.007$	0.003	0.007	NLO
$\Gamma(Z^0 \rightarrow had.)$	91.2	$0.130 \pm 0.012$	$0.130 \pm 0.012$	0.011	0.004	NNLO
$Z^0$ [ev. shapes]	91.2	$0.120 \pm 0.006$	$0.120 \pm 0.006$	0.001	0.006	NLO
$Z^0$ [ev. shapes]	91.2	$0.124 \pm 0.005$	$0.124 \pm 0.005$	0.001	0.005	resum.

Table 2: Summary of  $\alpha_s$  measurements

energy-energy correlations.<sup>47</sup> The resummed quantities remove the need to choose small renormalisation scales to fit the data, but the quoted error for resummed quantities still remains substantial.

#### 6.5. Summary on $\alpha_s$

Table 2, adapted from a summary by Bethke,<sup>45</sup> gives an overall view of the situation on  $\alpha_s$ . This information is also presented in graphical form in Fig. 8. This figure shows the efficacy of the various measurements in determining  $\Lambda$  and does not directly show the error on the determination of  $\alpha_s(M_Z)$ . The values of  $\alpha_s(M_Z)$  derived from these measurements are shown in Fig. 9.

#### References

1. P. Amaudruz et al., CERN-PPE-92-124 (July, 1992).
2. S.R. Mishra et al., Nevis Preprint NEVIS-1459, (June, 1992).
3. S. Fuess for the FFMF collaboration, this conference.
4. P. Berge et al. *Z. Phys.*C49 (1991) 187.
5. M. Virchaux, proceedings of *QCD at 20*, Aachen, 1992.
6. K. Bazizi and S.J. Wimpenny, preprint UCR-DIS-91-02.

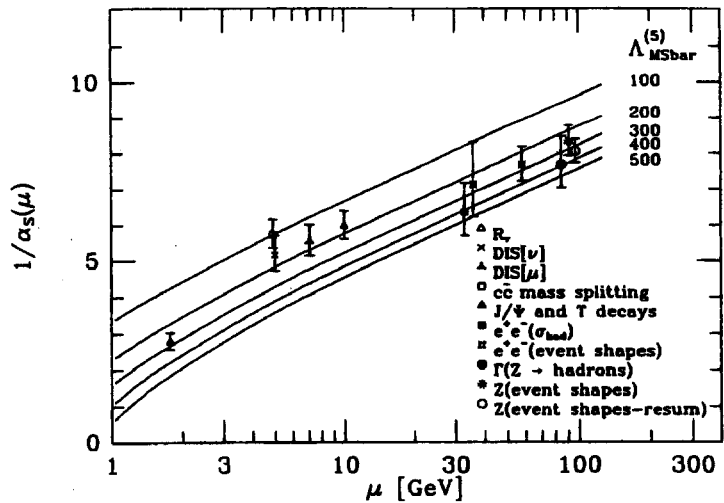


Figure 8:  $1/\alpha_s$  vs  $\ln \mu$

7. A.D. Martin, et al., Durham preprint, DTP-92-16 (Apr 1992) ;  
P.N. Harriman et al., *Phys. Rev. D*42 (1990) 798.
8. J.G. Morfin and W-K. Tung, *Z. Phys.*C52 (1991) 13 and private communication.
9. P. Amaudruz et al., *Phys. Rev. Lett.* 66 (1991) 2712.
10. E.J. Eichten et al, *Phys. Rev. D*45 (1992) 2269 and Fermilab-Pub-92/264-E,  
(1992).
11. P.B. Straub et al., *Phys. Rev. Lett.* 68 (1992) 452.
12. L.V. Gribov et al., *Phys. Rep.* 100 (1983) 1.
13. see, for example, G. Altarelli., *Phys. Rep.* 81 (1982) 1.
14. see for example, L.N. Lipatov in *Perturbative Quantum Chromodynamics*, World  
Scientific, A.H. Mueller, editor.
15. G. Marchesini and B.R. Webber, *Nucl.Phys.*B386 (1992) 215.
16. A.H. Mueller and H. Navelet, *Nucl.Phys.*B282 (1987) 727;  
J. Kwiecinski et al., *Phys. Rev.*D46 (1992) 921.
17. A.H. Mueller and J-W Qiu, *Nucl.Phys.*B268 (1986) 427
18. J. Kwiecinski et al., *Phys. Rev.*D44 (1991) 2640.
19. E.M. Levin, these proceedings;  
E.M. Levin et al., DESY-92-047 (March 1992);

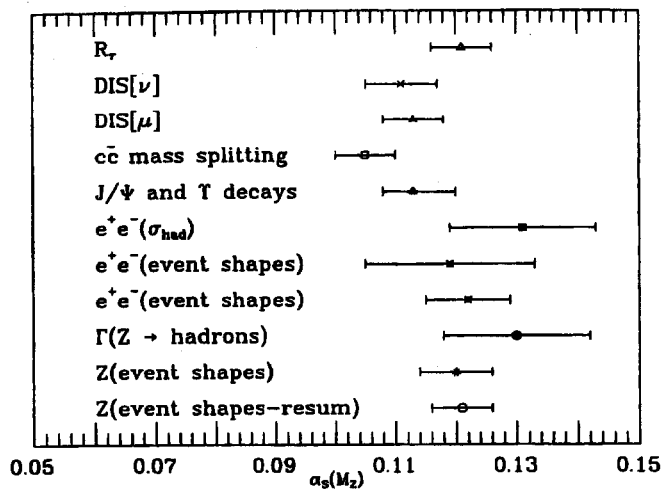


Figure 9:  $\alpha_s(M_Z)$

- J. Bartels, DESY-92-114 (August 1992).
20. J.M. Dunlea, this conference.
  21. J-W Qiu, this conference.
  22. G.R. Snow for the D0 collaboration, this conference;  
P. Maas for the CDF collaboration, this conference.
  23. H. Baer, J. Ohnemus and J.F. Owens, *Phys. Rev.D42* (1990) 61,  
J.F. Owens, private communication.
  24. J. Dunlea for the E706 collaboration, this conference.
  25. J. Appel, Fermilab-Pub-92/49, (1992).
  26. M. Aguilar-Benitez et al., *Nucl.Phys.B161* (1985) 400.
  27. G.A. Alves et al, Fermilab-Pub-92/208-E, (1992);
  28. T. Fuess, for the CDF collaboration, this conference;  
B.T. Huffman, for the CDF collaboration, this conference;  
S. Vejcik, for the CDF collaboration, this conference.
  29. P. Nason et al., *Nucl.Phys.B327* (1989) 49.
  30. C. Albajar et al., *Phys. Lett.B213* (1988) 405.
  31. E.L. Berger et al., Argonne preprint, ANL-HEP-CP-92-79.
  32. R.K. Ellis and D.A. Ross, *Nucl.Phys.B345* (1990) 79;

- J.C. Collins and R.K. Ellis, *Nucl.Phys.B360* (1991) 3;  
E.M. Levin et al., *Sov.J.Nucl.Phys.54* (1991) 867;  
S. Catani et al., *Nucl.Phys.B366* (1991) 135.
33. R.K. Ellis, *Phys. Lett. B259* (1991) 492 and references therein.
  34. E. Laenen et al., *Nucl.Phys.B369* (1992) 543.
  35. F.A. Berends et al., Fermilab-Pub-92/196-T, (1992).
  36. R.K. Ellis and S. Parke, Fermilab-Pub-92-132-T (May 1992).
  37. S.D. Ellis et al., *Phys. Rev. Lett. 69*(1992) 1496;  
H. Baer et al., *Phys. Lett. B234* (1990) 127;  
M.L. Mangano et al., *Nucl.Phys.B373* (1992) 295.
  38. W.T. Giele et al., Fermilab-Conf-92/213-T, (1992).
  39. J. Conrad for the E665 collaboration, this conference.
  40. E. Braaten et al., *Nucl.Phys.B373* (1992) 581.
  41. W. Marciano and A. Sirlin, *Phys. Rev. Lett.61* (1988) 1815.
  42. L.R. Surguladze et al., *Phys. Rev. Lett. 66* (1991) 560;  
S. Gorishny et al., *Phys. Lett. B259* (1991) 144.
  43. A. Pich, CERN-TH 6738/92 (1992).
  44. A. El-Khadra et al., *Phys. Rev. Lett. 69* (1992) 729.
  45. S. Bethke, Heidelberg preprints, HD-PY 92/12,92/13.
  46. S. Catani, et al., *Phys. Lett. B269* (1991) 432.
  47. S. Catani, et al., *Phys. Lett. B263* (1991)491;  
*Phys. Lett. B272* (1991)368;